Eulerian and Lagrangian Isopycnal Eddy Diffusivities in the Southern Ocean of an Eddying Model

A. GRIESEL

KlimaCampus, University of Hamburg, Hamburg, Germany

J. L. MCCLEAN, S. T. GILLE, AND J. SPRINTALL

Scripps Institution of Oceanography, University of California, San Diego, San Diego, California

C. EDEN

KlimaCampus, University of Hamburg, Hamburg, Germany

(Manuscript received 16 February 2013, in final form 27 October 2013)

ABSTRACT

Lagrangian isopycnal diffusivities quantify the along-isopycnal mixing of any tracer with mean gradients along isopycnal surfaces. They are studied in the Southern Ocean of the 1/10° Parallel Ocean Program (POP) model using more than 50 000 float trajectories. Concurrent Eulerian isopycnal diffusivities are estimated directly from the eddy fluxes and mean tracer gradients. Consistency, spatial variation, and relation to mean jets are evaluated. The diffusivities are calculated in bins large enough to reduce contributions from the rotational components that do not lead to net tracer mixing. Because the mean jets are nonzonal and nonparallel, meridional dispersion includes standing eddies and is significantly different from cross-stream dispersion. With the subtraction of the local Eulerian mean, the full Lagrangian diffusivity tensor can be estimated. Along-stream diffusivities are about 6 times larger than cross-stream diffusivities. Along-streamline averages of Eulerian and Lagrangian isopycnal diffusivities are similar in that they are larger north of the Antarctic Circumpolar Current (ACC) and smaller in the ACC in the upper 500 m. Eulerian diffusivities are often twice as large as the Lagrangian diffusivities below 500 m. There is large longitudinal variability in the diffusivities and in their relation to the mean flow. In bins with one prominent jet, diffusivities are reduced at the surface in the jet and increased to the north and south of the jet. There is a local maximum at depths of 500–1000 m. In other bins where mean jets merge and diverge because of topography, there is no consistent relation of the diffusivities with the mean flow. Eulerian fluxes are upgradient in about 15% of the bins.

1. Introduction

Eddy-driven mixing and advection are of leading-order importance in regions such as the Southern Ocean, where eddy processes account for both the horizontal and vertical transfer of tracers across the Antarctic Circumpolar Current (ACC). Present-day climate models do not explicitly resolve eddy mixing. Instead, climate models rely on diffusive parameterizations to represent spatially and temporally varying eddy processes. Diffusivities can be quantified using both Eulerian and Lagrangian methods. The Lagrangian approach is based on the spreading of particles or floats as they follow the flow (Taylor 1921), whereas Eulerian diffusivities are quantified from Eulerian eddy tracer fluxes (e.g., Eden 2006). When estimates are based on tracer releases, a diffusivity can be calculated from the lengthening of tracer contours in an eddying flow (Nakamura 2001), or from the rate at which the area of the tracer grows over time (e.g., Ledwell and Watson 1991). These estimates may also be regarded as (semi)Lagrangian because they are obtained from the spread of a tracer as it follows the flow. Estimates of eddy diffusivities in the Southern Ocean have been calculated using all of these methods. However, considerable disagreement has been found in both their magnitudes and in their horizontal and vertical structures (Ferreira et al. 2005; Marshall et al. 2006; Eden 2006; Sallée et al. 2008; Smith and Marshall 2009;

Corresponding author address: Alexa Griesel, KlimaCampus, University of Hamburg, Bundesstrasse 53, 20146 Hamburg, Germany.
E-mail: alexa.griesel@zmaw.de

DOI: 10.1175/JPO-D-13-039.1

Shuckburgh et al. 2009b; Abernathey et al. 2010; Ferrari and Nikurashin 2010; Griesel et al. 2010; Naveira Garabato et al. 2011).

The goal of this study is to estimate isopycnal eddy diffusivities and their depth dependence from both Eulerian (eddy tracer fluxes) and Lagrangian (particle dispersion) quantities in a consistent manner and to interpret their respective differences. Isopycnal diffusivity quantifies the mixing of tracers along isopycnal surfaces and across mean isopycnal tracer gradients and is to be distinguished from the skew diffusivity that can be interpreted as quantifying the advection of properties, such as buoyancy, through an eddy velocity (see, e.g., Griffies 1998). For this analysis, more than 50 000 numerical floats were deployed in an eddying Parallel Ocean Program (POP) simulation. This deployment scheme significantly improved the horizontal and vertical coverage of the domain relative to an earlier experiment in which numerical floats were deployed more sparsely in space (Griesel et al. 2010). The float deployment number was dictated by the computational load placed on the POP code by the online float advection scheme that is three-dimensional, and float advection is calculated at each model time step. This online advection scheme is computationally more expensive than, for example, a two-dimensional offline advection method (e.g., Sallée et al. 2011). The online scheme has the important advantage of allowing floats to be advected by the fully temporally resolved three-dimensional velocity field. It also simplifies the sampling of Eulerian quantities at float positions. This is needed both to determine Eulerian diffusivities along float trajectories and to determine Eulerian means, which are needed to define the background float velocity field.

Lagrangian floats provide a means to test the applicability of the eddy diffusion model [see LaCasce (2008) for an overview]. Taylor (1921) showed that Lagrangian particles in isotropic and homogeneous turbulence spread diffusively for periods longer than the integral time scale, with a constant diffusivity calculated from the integral of the velocity autocorrelation. Davis (1987, 1991) refined the theoretical framework to allow both the mean flow and diffusivity to be spatially variable.

In an ocean with inhomogeneous, strong mean flows and with an eddy field of varying horizontal scale, one of the challenges is to find the asymptotic behavior of the velocity autocorrelation, which requires sufficiently long time lags (e.g., Bauer et al. 1998; Veneziani et al. 2004; Davis 2005; Griesel et al. 2010). Strong rotational components of the eddy field, which are found in vortices and meanders of the Lagrangian trajectories, lead to oscillations in the autocovariances (Berloff and McWilliams 2002a,b; Veneziani et al. 2005; Griesel et al. 2010). These rotational motions are not associated with net mixing and tend to appear when the floats pass through quasi-stationary eddies in the presence of strong mean flows. Griesel et al. (2010) showed that when time lags are long enough to average over the negative lobes in the velocity autocorrelation, then strong mean flows act as barriers to mixing, whereas if the time lag is too short, eddy mixing appears enhanced in regions of strong mean flow and high eddy kinetic energy. The relationship between negative lobes and eddy–mean flow interactions was explained in more detail by Klocker et al. (2012a). They treated the ocean as an equivalent barotropic fluid governed by the quasi–potential vorticity equation in the presence of a background mean flow, representing the forcing with a fluctuation–dissipation stochastic term. Then they were able to show explicitly that the Lagrangian velocity autocorrelation is composed of an exponentially decaying part and an oscillatory part that is directly dependent on the phase speed of the eddies relative to the mean flow.

Similarly, rotational parts of the Eulerian eddy tracer fluxes play no role in the divergence of the eddy tracer flux and bias the computation of Eulerian diffusivities from eddy fluxes and mean tracer gradients (Eden 2006; Eden et al. 2007a,b; Griesel et al. 2010). One way to estimate local Eulerian diffusivities is to subtract a physically meaningful rotational flux from the raw fluxes (Eden et al. 2007a).

Diffusivities inferred from Lagrangian floats are often highly correlated with eddy kinetic energy (EKE) (Krauss and Böning 1987; Lumpkin et al. 2002; Zhurbas and Oh 2004; Sallée et al. 2008), which in the case of the ACC results in local maxima of eddy diffusivity in its core (Sallée et al. 2008). On the other hand, strong currents can also act as mixing barriers (e.g., Bower et al. 1985), leading to small effective eddy diffusivities in the core of the ACC (e.g., Marshall et al. 2006; Naveira Garabato et al. 2011). Naveira Garabato et al. (2011) invoked mixing length arguments and found that the spatial distribution of the eddy length scales, rather than the eddy velocities or EKE, determines the spatial distributions of the eddy diffusivities in the Southern Ocean. However, Shuckburgh et al. (2009a,b) showed that at any given geographic location, the magnitude of the diffusivity seems to depend on the relative importance of the strength of the mean flow and EKE, respectively. Thus, previous results appeared to contradict each other, with high EKE coinciding with high diffusivities in observed Lagrangian data and with low diffusivities in tracer-based interpretations.

Some of the differing diffusivity estimates were reconciled by later studies. Griesel et al. (2010) partially explained the discrepancies by pointing out that Lagrangian

diffusivities are sensitive to the time lag used to integrate the Lagrangian velocity autocovariance (AC), and some previous studies probably did not select sufficiently long time lags. However, the float deployments used by Griesel et al. (2010) were limited, both in terms of number and spatial distribution, and did not resolve the ACC sufficiently well to distinguish regimes with strong and weak mean flows. Klocker et al. (2012b) were able to reconcile Lagrangian and semi-Lagrangian tracer-based estimates of eddy diffusivities using a construct whereby eddies were defined as the deviation from a constant zonal-mean flow, provided that the number of floats was sufficiently large. Similar surface distributions of Eulerian and tracer-based eddy diffusivities were obtained by Abernathey and Marshall (2013).

Linear theory predicts low diffusivities near the surface and high diffusivities at a critical depth where the ACC velocity approximately balances the Rossby wave phase speed (Green 1970; Smith and Marshall 2009). In the ocean, eddies are generally nonlinear (Chelton et al. 2007, 2011), interact, and thus have a finite decorrelation time scale. As discussed by Ferrari and Nikurashin (2010) and Naveira Garabato et al. (2011), once a finite eddy decorrelation time scale is introduced in the problem, the mean flow acts to suppress mixing, and critical layers can be interpreted as regions where mixing suppression is not observed. Further support for this concept was obtained by Klocker et al. (2012b,a) using a sufficiently large number of floats to examine eddies in a constant zonal-mean flow with an equivalent barotropic vertical structure. Recently, Riha and Eden (2011) detected mixing barriers in jets at the surface in both Eulerian and isopycnal Lagrangian diffusivity estimates in an idealized zonal channel. They also found an increase of diffusivity with depth beneath the jets. In their study, the Eulerian diffusivities were based on the meridional eddy fluxes of potential vorticity and of buoyancy, corresponding to the diffusivities in the Gent and McWilliams (1990) (GM) parameterization. Lagrangian estimates of diffusivities were generally smaller than the Eulerian estimates, particularly at the surface.

Here, we expand on the work of Riha and Eden (2011) by considering Lagrangian versus Eulerian isopycnal mixing processes in a more realistic high-resolution ocean model. This model generates nonzonal, nonparallel jets, which can be strongly influenced by topography. Zonal asymmetries, in the form of topography, have an impact on cross-stream transport: Thompson and Sallée (2012) and Sallée et al. (2011) recently showed that mixing is highly localized and enhanced in the lee of bathymetric features. We pursue the following main questions: 1) what is the depth dependence of the Lagrangian isopycnal diffusivities, and how does it depend on longitude? 2) Can we estimate Eulerian diffusivities from the bin-averaged eddy tracer fluxes that are comparable to the Lagrangian isopycnal diffusivities? Instead of explicitly subtracting rotational parts from the Eulerian eddy fluxes, we pose the following hypothesis: when the diffusive limit in the Lagrangian diffusivity is reached (i.e., when the time lag/bin size is large enough for the flow to be in the diffusive regime), we also expect the Eulerian fluxes averaged over the same bin size to represent a diffusive flux (i.e., we expect the Eulerian fluxes to have a net downgradient component without explicit subtraction of the rotational parts). This seemingly poses a contradiction to the study of Griesel et al. (2009) who found that rotational parts of the eddy fluxes dominate on all length scales and is another starting point for this paper. We show that provided bins are of sufficient extent and the local Eulerian mean velocity is subtracted, Lagrangian along- and cross-stream isopycnal diffusivities can be estimated. We also show that the Lagrangian diffusivities have vertical structures that are similar to the corresponding Eulerian isopycnal diffusivities obtained from along-streamline averages particularly in regions with distinct jets. Otherwise significant differences remain.

This paper is organized as follows: section 2 describes the Lagrangian float data and the requirements for bin sizes, as well as discussing the resulting Lagrangian diffusivity distributions. Section 3 describes how the Eulerian isopycnal diffusivities are computed, comments on the averaging scale necessary for the Eulerian eddy fluxes to have small rotational components, and compares the Lagrangian and Eulerian diffusivities. Section 4 contains the summary and conclusions.

2. Lagrangian diffusivities

In this section we describe the eddying ocean general circulation model used in the study, the model deployment strategy of Lagrangian parcels that are subsequently advected online through the simulated flow field, the methodology used to calculate Lagrangian diffusivities, and finally the dependence of the resulting diffusivities on coordinate system orientation and longitude.

a. Ocean model and methodology

We use the nominal 1/10° global POP model in a configuration described in detail by Maltrud et al. (2010). An earlier 1/10° POP simulation (Maltrud and McClean 2005) was used by Griesel et al. (2009, 2010). A notable difference to the previous configuration is that the grid has been changed from a dipole to a tripole layout. The vertical resolution is the same, but there

are two additional deep levels increasing the number of vertical levels to 42. Bottom topography is now discretized with partial bottom cells.

The initial condition used for our simulation is the 100-yr spun-up state of Maltrud et al. (2010) that was forced with monthly averaged ''normal year'' Common Ocean–Ice Reference Experiments (CORE) atmospheric fluxes constructed by Large and Yeager (2009). Normal year forcing represents climatological conditions constructed from 43 years of interannually varying atmospheric state; it is made up of single annual cycles of all the atmospheric fields needed to force an ocean model. The 6-hourly forcing was averaged to monthly forcing. Wind stress was calculated offline using bulk formulae and the Hurrell sea surface temperature (SST) climatology (Large and Pond 1982; Hurrell et al. 2008); evaporation and sensible heat flux were calculated online using the same bulk formulae and the model-predicted SST. Maltrud et al. (2010) provide more details of the forcing and model setup.

In the spun-up state, 56 000 floats were deployed in the Southern Ocean between latitudes 70° and 35°S with a spacing of 5° in longitude, 0.4°–0.8° in latitude, and 200 m with depth. The floats were advected by the three-dimensional model flow for 2 years using a fourth-order Runge–Kutta scheme at every model time step. Figure 1 shows the trajectories that lie in the 200–400-m depth range after 2 years of integration and the eddy kinetic energy field that they are sampling. The domain is well sampled, except in the most equatorward latitudes where coverage varies from basin to basin due to regional subtropical energetics. The day-to-day change in density that each float experiences is mostly smaller than the mean density change per meter depth (not shown), meaning that the floats do not deviate more than a meter from the mean density surface where they were located on the previous day. Another measure of the degree to which the floats follow isopycnals is the density difference after 30 days of travel. We choose 30 days because this is the time lag at which the diffusivities will be diagnosed (see section 2b). The mean density change for all floats originating in the upper 500 m is 0.058 ± 0.116 and $0.004 \pm 0.009\ \mathrm{kg\,m^{-3}}$ for the floats originating in the 500–1000-m depth range. Below about 500 m, away from mixed layers, lateral diffusion is orders of magnitude larger than diapycnal diffusion, and so we assume here that the lateral dispersion of the floats can serve as a measure of isopycnal diffusion.

The Lagrangian diffusivity κ^L is determined by the integral of the Lagrangian velocity autocorrelation function:

$$\kappa^L_{ij}(\mathbf{x},\tau) = \int_{-\tau}^{0} d\tilde{\tau}\langle u_i'(t_0\,|\,\mathbf{x},t_0)u_j'(t_0+\tilde{\tau}\,|\,\mathbf{x},t_0)\rangle_L, \quad (1)$$

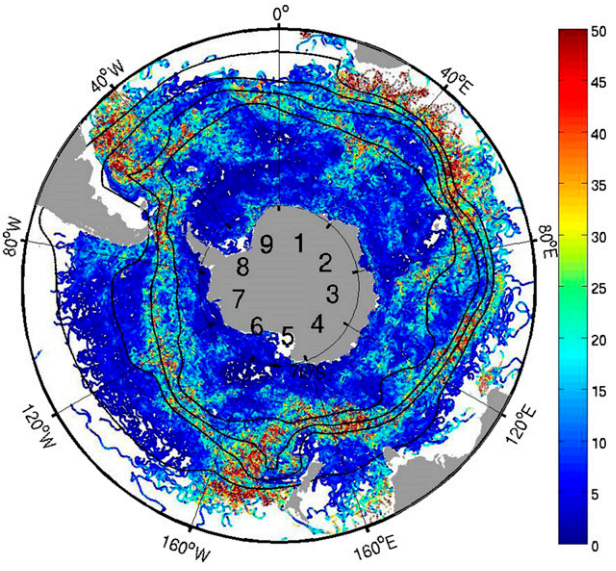

FIG. 1. Trajectories of floats in depth interval 200–400 m. Color is the square root of the Lagrangian eddy kinetic energy $\sqrt{u'^2+v'^2}$ ($\mathrm{cm\,s^{-1}}$), where u' and v' are the deviation of the Lagrangian zonal and meridional velocity from the Eulerian mean velocity at each float location, respectively. Also shown are four of the streamlines and nine lon segments used for binning in section 2.

where $u_i'(t_0+\tau\,|\,\mathbf{x},t_0)$ denotes the residual velocity of a particle at time $t_0+\tau$ passing through x at time t_0 (Davis 1987). The angle brackets denote the Lagrangian mean. The residual velocity is calculated as the deviation from the Eulerian mean velocity, and hence the single-particle diffusivity is a mixed Eulerian–Lagrangian quantity. If the diffusivity exists, that is, if the eddy field has a diffusive component, then for sufficiently long time lags, the integral converges to a constant κ^∞ that characterizes the time-mean dispersion for long time lags.

The approach taken by Davis (1987), strictly speaking, is valid for an ensemble of particles passing through a fixed position at different moments in a shear flow. In practice, particles do not all pass through exactly the same point, and instead we consider an ensemble of particles taken from a finite area (or bin) in a shear flow. The time-mean Eulerian flow in the ACC consists of multiple jets whose cross-stream scale is comparable to the eddy scale. As shown by Oh et al. (2000), in a shear flow the along-stream diffusivity is affected by the shear dispersion. If we remove a spatially uniform average from each float velocity, we are left with a residual due to the mean shear that may dominate the diffusivity estimate (Bauer et al. 1998; Koszalka et al. 2011). When Griesel et al. (2010) subtracted the local mean instead of a spatially uniform mean, their resulting Lagrangian diffusivities were characterized by good convergence properties, a result of minimizing the influence of shear dispersion.

b. Results from Lagrangian deployments: Bin sizes and dependence on time lag

The simulated Lagrangian diffusivities were calculated using trajectories in fixed bins. In the vertical direction we used 200-m spacing, resulting in 14 bins. In the meridional direction we used along-stream binning constructed from the model's time mean and spatially filtered barotropic streamlines $\Psi_g = gf^{-1}\eta$, where η is the time-mean model sea surface height (SSH), g is the gravitational acceleration, and f is the Coriolis parameter. Barotropic streamlines are dynamically more consistent than zonal contours, as they are aligned with mean ACC jets, at least at the surface. The raw unfiltered 3-year-mean streamlines cannot be used for binning due to their convoluted complex structure and because their paths are a nonunique function of latitude. On the other hand, spatial filtering may lead to floats oscillating between bins particularly in the lee of topographic features with small-scale standing meanders. Here we define cross- and along-stream Lagrangian diffusivities (see section 2c) using the local depth-dependent Eulerian mean velocities, which are different from the depth-independent velocities derived from the barotropic streamlines and are an unfiltered representation of cross-stream dispersion. The barotropic streamlines define the zonal integration path for along-streamline averages. As discussed by Viebahn and Eden (2012), an isopycnal meridional overturning circulation with an exactly vanishing standing eddy part should be computed by zonally integrating along depth-dependent horizontal isolines of time-mean density. However, neglecting the depth dependence of the zonal integration paths by integrating along geostrophic streamlines of a fixed depth may represent an acceptable approximation (Viebahn and Eden 2012).

The along-stream bin size needs to be large enough that the trajectory segments in the bin are each sufficiently long that the diffusivity converges and is representative of that bin (and not of the neighboring bins). In regions of the ACC where large velocities occur, the floats will be advected quickly downstream; large velocities also correspond to closely spaced streamlines, meaning that floats are prone to leave the bins in the meridional direction. Table 1 assesses the number of days the floats stay in the bins for different meridional and longitudinal grid spacings. Zonal spacing can be decreased at the expense of meridional spacing increase. For a longitudinal grid spacing of 40° and a streamline binning of $\Delta\Psi_g = 1 \times 10^4\,\mathrm{m^2\,s^{-1}}$, most floats stay in the bins for 30 days, whereas when the longitudinal bin size is reduced to 20° the meridional spacing needs to be doubled for most floats to stay in the bins for more than 30 days.

TABLE 1. Mean number of days that a float stays in each bin in the along-stream average at 300-m depth is shown in the middle column. The bin size is expressed as spacing in lon (°) times spacing in streamline ($10^4\,\mathrm{m^2\,s^{-1}}$) in the left column. The error bars are the std dev for the along-stream average. Percentage of bins where the mean number of days is smaller than 30 days is shown in the right column.

Bin size	Mean number of days	% bins < 30 days
10° × 1	17 ± 11	50%
10° × 2	26 ± 15	33%
20° × 1	23 ± 14	46%
20° × 2	37 ± 19	22%
40° × 1	30 ± 13	37%

We now examine the Lagrangian diffusivity as a function of time lag to determine the time lag at which the Lagrangian diffusivity converges. In the cross-stream direction, diffusivity oscillates with time lag (Fig. 2a), and there is a significant difference between the peak diffusivity occurring between lags of 0–10 days, and that occurring for lags >30 days. This difference decreases with depth (Fig. 2b). The ratio of the maximum diffusivity and that diagnosed at time lags >30 days also decreases with depth. On average, this ratio is about 3 at 500-m and about 1.7 at 1300-m depth. Circling and meandering trajectories do not lead to any net cross-stream dispersion, and as a result the diffusivity as a function of time lag oscillates before it converges to the correct value of diffusivity (Griesel et al. 2010). This is consistent with the ideas discussed by Klocker et al. (2012b,a). They report that at the surface, eddies propagate relative to the mean flow so that their overall speed becomes smaller than the mean flow speed, and the eddies appear quasi stationary. Floats at the surface are advected through these quasi-stationary eddies, leading to oscillating autocorrelations, and so the eddies do not have time to disperse the floats. At depth, eddies tend to move at similar speeds to the mean flow and have time to mix.

In contrast, in the along-stream direction there is no oscillatory behavior because along-stream advection dwarfs oscillatory motions. If the local Eulerian mean is not subtracted, dispersion grows in the along-stream direction (Figs. 2e,f). However, when the local Eulerian mean is subtracted, convergence improves, and the along-stream diffusivity can be determined, particularly deeper in the water column (Fig. 2d).

The behavior of the diffusivity as a function of time lag (Fig. 2) shows that in the case of the cross-stream diffusivities the diffusive limit can be reached in 30 days; however, for the along-stream diffusivities, a minimum of 50 days is required. Because our emphasis is on the cross-stream Lagrangian diffusivity, based on Table 1 and Fig. 2, we decided to use the bin sizes listed in the

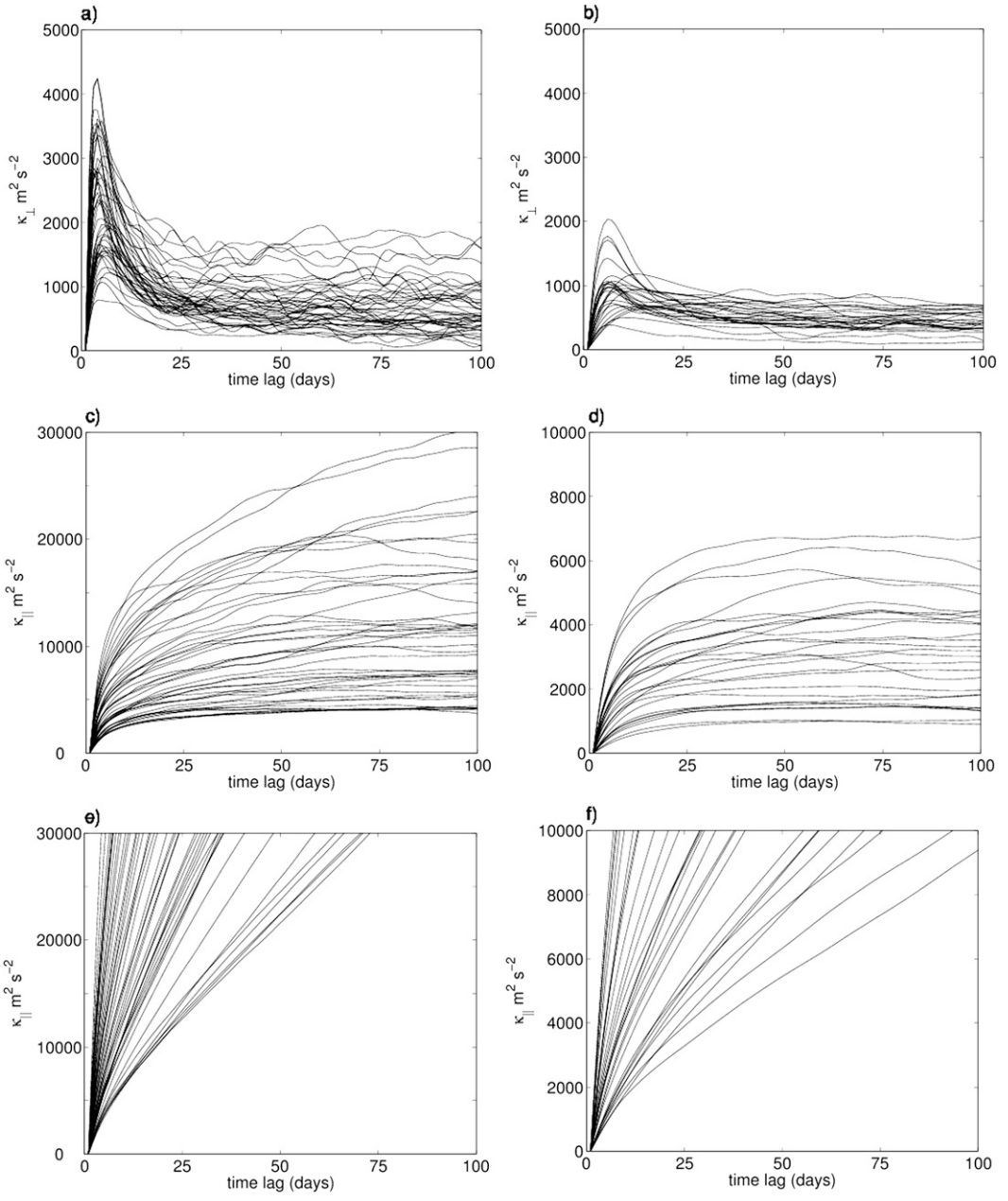

FIG. 2. Cross-stream diffusivity as a function of time lag in the core of the ACC for bins at (a) 300 and (b) 1500 m. (c),(d) As in (a),(b), but for along-stream diffusivity. (e),(f) Along-stream diffusivity as in (c),(d), but without subtraction of the Eulerian mean. Note the different scales on the *y* axes.

last two rows of Table 1. In section 2c, we focus on meridional variability by using 40° longitude in the zonal direction and meridional spacing defined by barotropic streamline contours with $\Delta\Psi_g = 1 \times 10^4\,\mathrm{m^2\,s^{-1}}$. This results in 15 bins in the meridional direction. In section 3, we focus on longitudinal variability by using a barotropic streamline spacing of $\Delta\Psi_g = 2 \times 10^4\,\mathrm{m^2\,s^{-1}}$ and a longitudinal grid size of 20° overlapping by 5°, leading to 72 bins in the longitudinal direction. Note that bin sizes here are larger than typically used in earlier studies (e.g., Sallée et al. 2008).

c. Lagrangian diffusivity distributions

For homogeneous statistics and negligible shear dispersion, the Lagrangian diffusivity tensor is symmetric, and therefore can be diagonalized with $\mathbf{K} = E\mathbf{\Lambda}E^{\mathrm{T}}$, where E contains the eigenvectors of $\mathbf{K}$ and $\mathbf{\Lambda}$ is the diagonal matrix containing the eigenvalues λ_i. We computed $\mathbf{K}$ in a

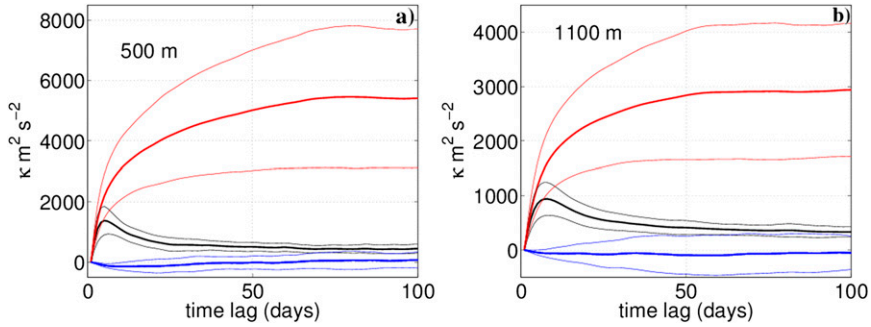

FIG. 3. Lagrangian diffusivity tensor components as a function of time lag in along-streamline average for a depth of (a) 500 and (b) 1100 m and mean lat 52°S: black is $\kappa_{\perp}$, magenta is $\kappa_{\parallel}$, and blue is $\kappa_{\perp\parallel}$. Also shown in thin lines is the std dev of the along-streamline average.

coordinate system projected along and across the Eulerian mean velocity; hence, the off-diagonal components of **K** are indistinguishable from zero (Fig. 3). However, the two eigenvalues, $\lambda_{\perp}$ in the cross- and $\lambda_{\parallel}$ in the along-stream direction, are not equal. The along-stream diffusivity is larger by a factor of about 6 than the cross-stream diffusivity at 500- and 1100-m depth in the along-streamline average.

1) Dependence on coordinate system orientation

Classically, Lagrangian diffusivity has been quantified in a zonally meridionally oriented coordinate system, but other coordinate systems have also been explored, such as across- and along-f/H contours where H is ocean depth (LaCasce 2000), across-bin mean streamlines (Sallée et al. 2008), and across the local Eulerian time mean (Griesel et al. 2010). The depth dependence of Lagrangian diffusivity in the Southern Ocean has previously been explored in the meridional direction, implying that eddies were defined as deviations from the zonal-mean jets (e.g., Riha and Eden 2011; Klocker et al. 2012b). The model used by Riha and Eden (2011) did not include topography, so meridional dispersion did not include a standing eddy component, but in studies where the influence of topography is not explicitly excluded, the definition of eddies as the deviation from the zonal mean can include a standing eddy contribution.

In our study, we show that the depth variation of Lagrangian diffusivity differs depending on the coordinate system orientation. Figure 4 shows the depth dependence of the along-stream average of meridional (blue line) and cross-stream (red line) eddy diffusivity in the ACC core. In both cases, diffusivities are diagnosed at a time lag of 30 days. To compute the cross-stream eddy diffusivity (red profile), the Lagrangian velocities are projected across the Eulerian mean velocity. For Fig. 4 we used the streamline bin with the maximum along-streamline average Eulerian mean velocity, which corresponds to an average latitude of 50°S. Meridional Lagrangian diffusivity decreases rapidly from 6800 ± 642 $m^2 s^{-1}$ near the surface to 3000 ± 150 $m^2 s^{-1}$ at 1500-m depth and is about 6 times larger near the surface than the Lagrangian diffusivity. This difference indicates that the meridional dispersion still contains a substantial contribution from the along-stream component of isopycnal diffusivity, which can be interpreted as a measure of the deviation of the Eulerian mean jets from a zonal orientation. Because the averages are based on 40°-long bins, deviations from the zonal direction over this scale contribute to the differences between meridional and cross-stream diffusivities. The along-stream diffusivity (calculated in section 2b) is about 6 times larger than the

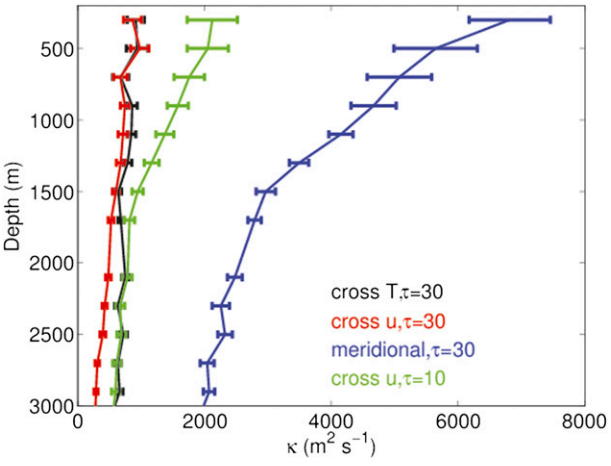

FIG. 4. Along-streamline average of meridional and cross-stream diffusivity as a function of depth in the core of the ACC. Shown is the streamline bin with the max along-streamline average Eulerian mean velocity corresponding to an average lat of 50°S: Lagrangian velocity is projected across mean temperature contours (black) and across the Eulerian mean velocity, and the diffusivity is diagnosed at time lag 30 (red) or 10 (green) days. The blue line is the Lagrangian diffusivity diagnosed from the Lagrangian meridional velocity.

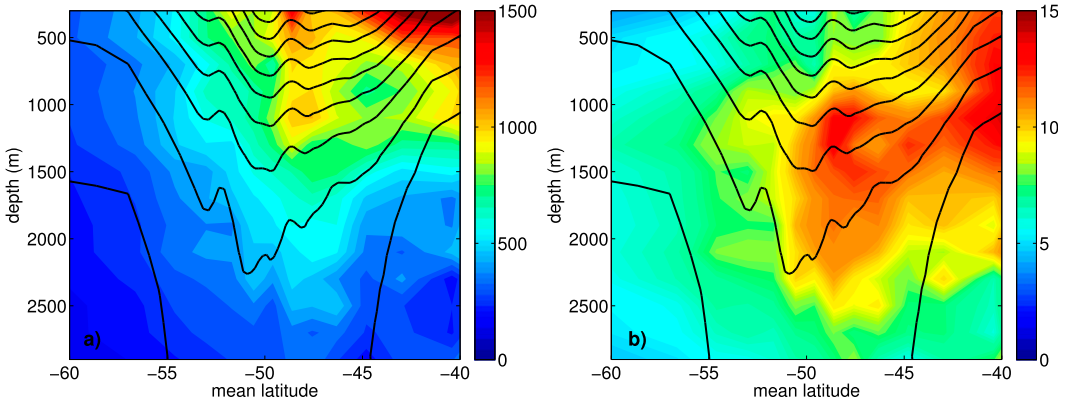

FIG. 5. (a) Along-streamline average of Lagrangian diffusivity ($m^2\,s^{-1}$). The profile around 50°S corresponds to the red line in Fig. 4. (b) Along-streamline average of Lagrangian integral length scale (km). Contours are Eulerian-mean velocity averaged along the streamline bins with a contour interval of $2\,cm\,s^{-1}$.

cross-stream diffusivity (Fig. 3) and is highly correlated with eddy kinetic energy that decreases with depth (cf. Figs. 2c,d).

In section 3a, we will quantify the Eulerian diffusivity as diffusion across mean temperature contours. For the most consistent comparison with the Eulerian diffusivity, we also consider the projection of the Lagrangian velocity across mean potential temperature Θ contours in section 3 (black line in Fig. 4). For both cross-stream and cross-$\overline{\Theta}$ contour frameworks with diffusivity diagnosed at a time lag of 30 days, κ^L is on the order of 500–700 $m^2\,s^{-1}$ and is quite uniform with depth in the along-streamline average (red and black lines in Fig. 4). This is consistent with previous findings of Griesel et al. (2010). In the upper ocean, mean temperature contours and velocities are better aligned than they are below depths of 1500 m, where the two diffusivities differ.

The vertical dependence of κ^L also depends on the time lag at which it is diagnosed. Diffusivities are twice as large in the upper 1000 m when the time lag is too short (green line in Fig. 4), because the short lag diffusivity is not representative of κ^∞, as discussed in section 2b and in Griesel et al. (2010).

The Lagrangian diffusivity can be written as

$$\kappa^L = \sqrt{\langle u'^2 \rangle} L_L, \tag{2}$$

where L_L is the Lagrangian eddy "length scale" that is obtained from the area under the integral of the velocity AC, normalized by the square root of the AC at zero lag: $L_L = 1/\sqrt{R_L(0)} \int_0^\infty R_L(\tau)\, d\tau$. Here $\sqrt{\langle u'^2 \rangle}$ is the square root of the Lagrangian eddy kinetic energy, where the prime is the deviation of the Lagrangian velocity from the Eulerian mean at each float location. In theory, with an exponentially decaying velocity AC, L_L quantifies the length after which the float velocities are no longer correlated and can be assumed to conform to a random walk regime. In practice, in the presence of mean flows, eddy–mean flow interactions lead to oscillations in the velocity AC between positive and negative values (Griesel et al. 2010; Klocker et al. 2012b,a). This means that the Lagrangian integral scale cannot be interpreted as a meaningful decorrelation scale. Figure 5a shows the along-streamline average of the cross-stream Lagrangian diffusivity as a function of latitude and depth and Fig. 5b shows the effective Lagrangian length scale obtained from the integral of the velocity AC after 30 days. The mixing barrier effect of the mean flow is apparent in the upper 1000 m (south of about 45°S) where significant negative lobes in the velocity AC reduce the effective length scale to less than 10 km. The combination of this increase of the length scale with depth and the strong decrease of EKE with depth (not shown) leads to Lagrangian diffusivities of about 700–1200 $m^2\,s^{-1}$ in the upper ACC, increasing to 1500 $m^2\,s^{-1}$ on the northward flanks in the upper 500 m (Fig. 5a).

2) LONGITUDINAL VARIABILITY

The ACC consists of multiple jets whose positions and strengths vary considerably with longitude (see Fig. 6). The intensity of the jets varies along the streamlines and the individual branches merge and diverge, often in response to interactions with bathymetry. Although the fronts change position and intensity with time, Sokolov and Rintoul (2009) concluded from a time series of SSH observations that the jets are aligned with particular streamlines along the circumpolar path of the ACC. In POP, the time-mean ACC jets are not consistently associated with single SSH contours along the entire circumpolar path. Consequently, the along-streamline average combines stronger and weaker mean flow

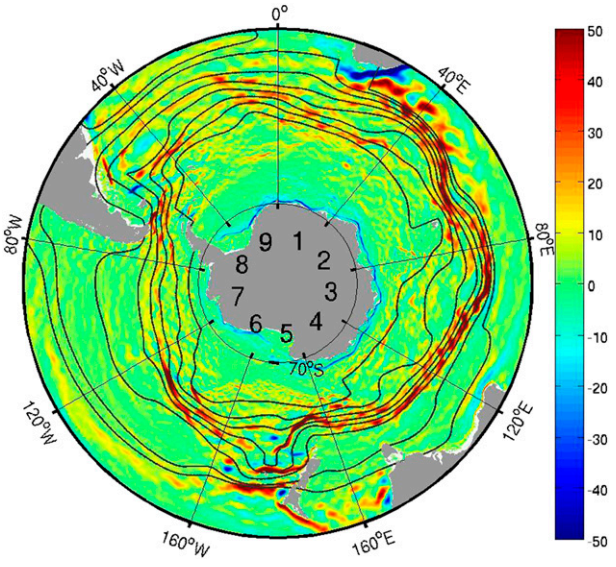

FIG. 6. Eulerian-mean velocity at 300-m depth ($\mathrm{cm\,s^{-1}}$) and every other streamline used for binning. The streamline spacing is $\Delta\Psi_g = 2 \times 10^4\,\mathrm{m^2\,s^{-1}}$. Also shown are the nine lon segments used for binning in section 2.

regimes with corresponding stronger or weaker mixing barriers. The uniform depth distribution of cross-stream Lagrangian diffusivities shown in Fig. 4 arises from along-stream averaging, but this does not mean that Lagrangian diffusivity is uniform with depth in all bins. Figure 6 shows that when the dominant flow is confined to a single jet (as in bins 3 and 6 in Fig. 6), and associated with the same streamlines, then the cross-stream Lagrangian diffusivity exhibits a spatial structure to be expected from critical layer theory. Evidence of a mixing barrier is seen in the jet at depths less than 1000 m in both bin 3 (Fig. 7a) and bin 6 (Fig. 7b); below this level diffusivity increases with depth in the jet as well as on its northern and southern flanks.

When the ACC flow is distributed between multiple jets (as in bins 5 or 8 in Fig. 6), mixing barriers are less evident. Streamlines are influenced by topography, and the jet structures are more complex, making it difficult to resolve spatial variations due to limitations arising from the bin size requirements. Bin 8, around the Drake Passage (Fig. 7c), exhibits two jets with mixing barriers within the jets and enhanced mixing in between. However, there is no evidence of a mixing maximum at a depth below the jets. Instead, diffusivity decreases with depth. Bin 5, encompassing New Zealand (Fig. 7d), contains regimes of high and low flow and even westward jets within a single streamline bin. The complexity added by eddy, jet, topography interactions in this bin leads to a diffusivity distribution that cannot be interpreted in a straightforward manner.

3. Eulerian–Lagrangian comparison

In this section, we describe the methodology used to calculate Eulerian diffusivities. Lagrangian and Eulerian diffusivities are then compared and their differences are discussed.

a. Method

Davis (1991) showed that in inhomogeneous flows with finite-scale eddies, the evolution of the mean tracer concentration depends only on the initial conditions of the mean and source fields and the single-particle statistics. As discussed in section 2a, if the time lag τ goes to infinity, or rather, is greater than some time T that reflects the finite scales of the dispersing eddies, $\kappa(x, t)$ approaches a constant value κ^{∞}, and the eddy flux is approximated by the typical advection–diffusion equation

$$\langle u_i'(\mathbf{x},t)\Theta'(\mathbf{x},t)\rangle = -\kappa_{ij}^{L\infty}(\mathbf{x})\partial_{x_j}\overline{\Theta}(\mathbf{x},t), \qquad (3)$$

where Θ is a tracer concentration, and $\kappa_{ij}^{L\infty}$ is the Lagrangian diffusivity tensor defined in Eq. (1) when the time lag approaches infinity. The angle brackets are the average over the Lagrangian bin.

To compute the Eulerian eddy diffusivities from the eddy fluxes themselves, the horizontal eddy flux of the tracer Θ can be decomposed into three terms: a component perpendicular to the mean tracer contours, involving the (scalar) Eulerian diffusivity κ^E; a component that is along the mean tracer gradient with a streamfunction B characterizing eddy advective effects; and a rotational part with vector potential $\mathbf{C}$ that serves as a gauge potential. The gauge potential does not affect the divergence of the eddy flux, but it does affect the definition of κ and B (e.g., Eden et al. 2007b):

$$\overline{\mathbf{u}_\mathbf{h}'\Theta'} = -\kappa^E\nabla\Theta - B(\mathbf{k}\times\nabla_h\Theta) + \mathbf{k}\times\nabla_h\mathbf{C}. \qquad (4)$$

Equation (4) is the decomposition of the horizontal eddy flux on constant z levels. However, because the Lagrangian floats travel along isopycnals and measure the isopycnal diffusion, the Eulerian diffusivity κ^E is calculated as

$$\kappa_\rho^E = -\frac{\langle F_{\rho\perp}\rangle}{\langle|\nabla_\rho\Theta|\rangle}, \qquad (5)$$

where $F_{\rho\perp}$ is the isopycnal eddy flux across mean-Θ contours and $|\nabla_\rho\Theta|$ is the isopycnal-mean Θ gradient, that is, the part of the Θ gradient that is directed along the local isopycnal surface. The angle brackets denote an average along the float trajectories. Note that this isopycnal diffusivity is to be distinguished from the diffusivity used in the GM parameterization, which is

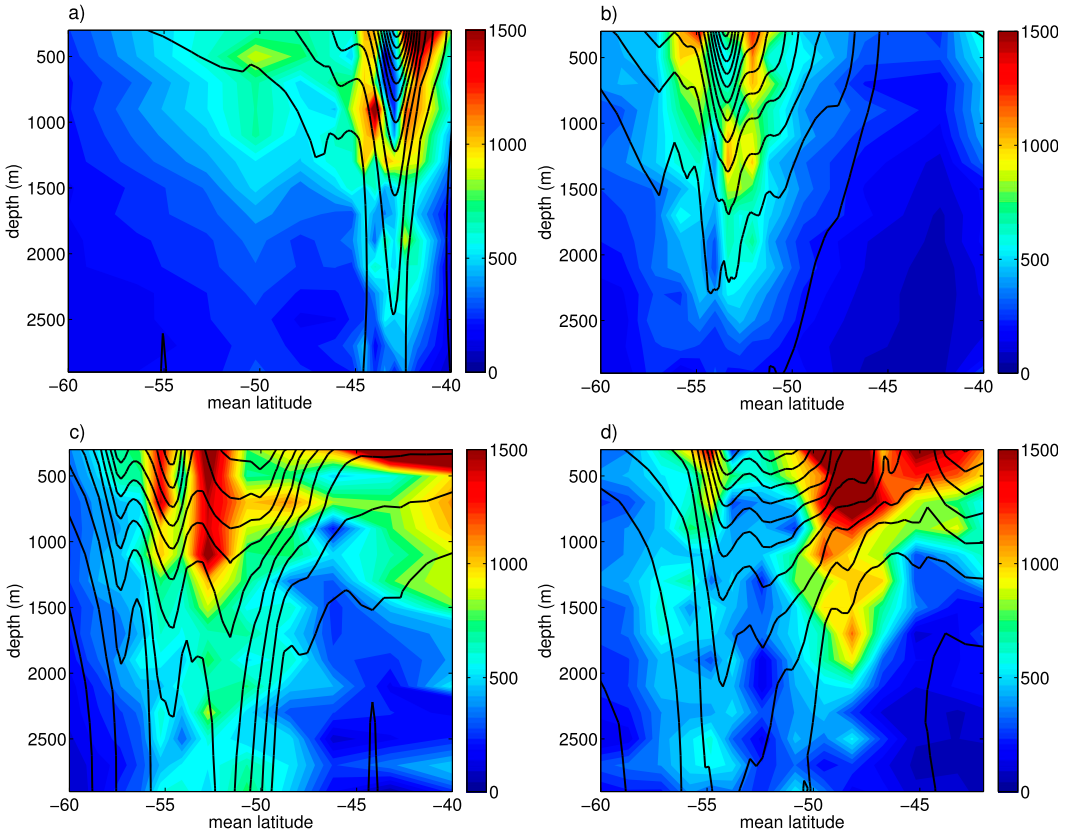

FIG. 7. Lagrangian cross-stream diffusivity as a function of depth and latitude ($m^2 s^{-1}$). Bins (a) 3, (b) 6, (c) 8, and (d) 5 from Fig. 6. Contours are Eulerian mean velocity averaged along the streamline bins.

calculated from the horizontal eddy buoyancy flux and the horizontal buoyancy gradient (Smith and Marshall 2009; Vollmer and Eden 2013; Abernathey et al. 2013).

b. *Eulerian bin size requirements*

As part of the computation of Eulerian diffusivity κ^E, an appropriate bin size needs to be chosen as indicated by the angle brackets in Eq. (5); constraints on this choice are discussed in this section.

In the Southern Ocean, a large part of the eddy flux circulates along contours of eddy variance, as shown in Fig. 8a for a region west of the Drake Passage. The rotational component [represented by **C** in Eq. (4)] can be related to advection and time evolution terms in the eddy variance equation (see, e.g., Marshall and Shutts 1981; Eden et al. 2007a). These rotational parts locally lead to oscillations between up- and downgradient eddy fluxes that we expect to average out over large enough scales. In the global average, the advective terms vanish completely. In the zonal average, when there is no mean meridional flow, only the triple correlation and time evolution terms contribute to the rotational flux. If those two contributions are small, then the diffusivity calculated from the raw zonally averaged flux is equivalent to the diffusivity calculated after the subtraction of the rotational parts. This was shown, for example, in appendix C of Abernathey and Marshall (2013).

Abernathey and Marshall (2013) show that variance advection occurs mostly on scales below 500 km, meaning that variance is dissipated within 500 km of where it is produced. Provided that the averaging interval (i.e., the bin) is large enough, we expect, on average, a net downgradient flux. This point is illustrated in Fig. 8b, which shows the large variation of the eddy heat flux along three float trajectories. The heat flux, when averaged along each of the three trajectories, tends to converge after about 40 days to a constant downgradient value, about an order of magnitude smaller than the local heat flux, in all cases. This is similar to finding a diffusive limit for κ^L at large time lags (and large bin sizes). For the Lagrangian diffusivity, oscillations on time scales less than about 40 days represent the rotational parts. Hence, just as in the original work of Taylor (1921), if the diffusive limit is reached the bin-averaged eddy flux can be interpreted as a diffusive parameterization. As was shown in Table 1, a bin size of 20°

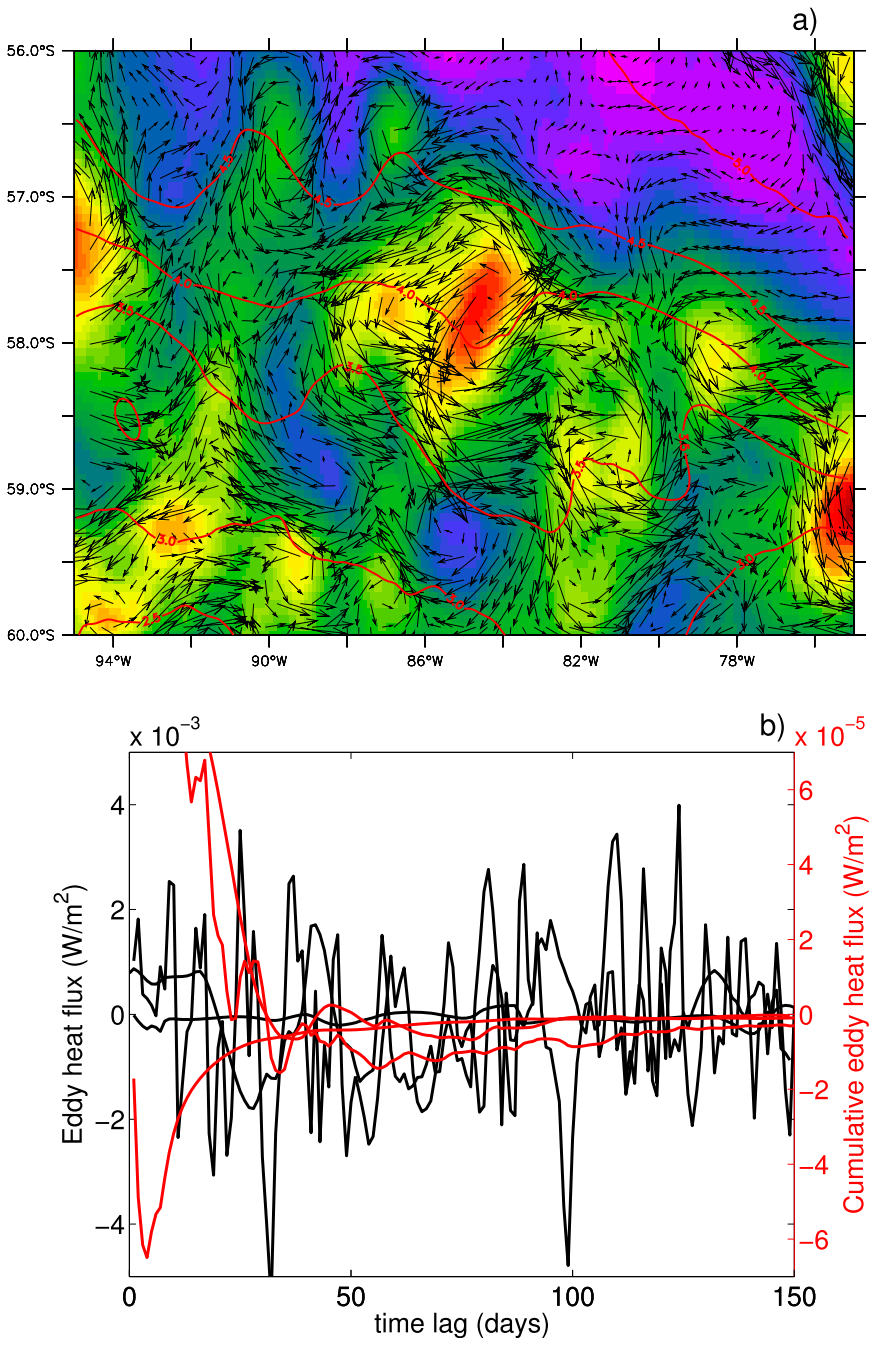

FIG. 8. (a) Horizontal eddy flux (vectors; $\mathrm{W\,m^{-2}}$), eddy variance $\overline{\Theta'^2}$ (color; $^\circ\mathrm{C}^2$), and $\overline{\Theta}$ (contours; °C) for a region west of the Drake Passage. (b) Cross-stream eddy heat flux along three trajectories (black, left axis; $\mathrm{W\,m^{-2}}$) and associated cumulative mean cross-stream heat flux averaged along each trajectory (red, right axis; $\mathrm{W\,m^{-2}}$).

longitude means that most floats stay in the bin for more than 30 days during which time the Lagrangian diffusivity converges.

We note here that our choice of averaging scale seems to contradict the outcome of Griesel et al. (2009), who concluded that rotational parts dominate on all scales. However, their analysis was based on zonal and not along-streamline averaging scales and only for limited regions. We may expect rotational parts to average out more when following the flow. We find here that the κ^E when calculated from along-streamline averaged fluxes and gradients are the same as when the κ^E are calculated

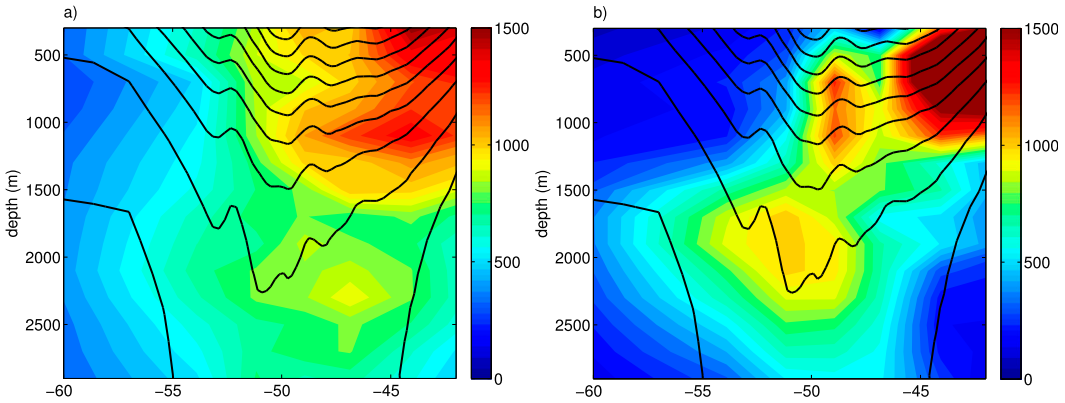

FIG. 9. Along-stream averages of diffusivities as a function of depth and lat averaged over the bin for each streamline bin. (a) Lagrangian and (b) Eulerian diffusivities ($m^2 s^{-1}$). Contours are Eulerian mean velocity averaged along the streamline bins.

in the 20° bins and then averaged. This suggests that the averaging length scale may be long enough for most bins, but not for all bins because, as we note below, κ^E are sometimes negative. We now proceed to report results from the Eulerian experiments based on our hypothesis that the averaging scale is sufficient as determined by the requirements of Lagrangian diffusivity convergence.

c. *Eulerian diffusivity distributions*

We now compare κ^E with κ^L. Because κ^E quantifies along-isopycnal diffusion across the mean temperature contours, to obtain consistent comparisons we also project the Lagrangian velocities across the mean temperature gradient (see also the black line Fig. 4), rather than projecting them across the Eulerian mean velocity.

The along-stream averages of the 20° longitude, binned κ^E and κ^L are shown in Fig. 9. Common features are that both diffusivities are high toward the northern flanks of the ACC, and lower in the ACC. However, north of 45°S, κ^E (Fig. 9b) is roughly double κ^L (Fig. 9a), while to the south of 45°S above the depths of about 700 m, κ^E is lower than κ^L in the along-stream average. Thus, the local maximum of diffusivities around 1000-m depth is more distinct and larger in the Eulerian case than in the Lagrangian case. For both κ^E and κ^L, another local maximum occurs around a depth of 1500–2500 m, although the maximum is several degrees farther northward in the κ^L case (Fig. 9). This maximum is a result of the projection across temperature contours, because it does not appear in the projection across the Eulerian mean velocity (Fig. 5). At depths between 1500 and 2500 m, both mean flow and EKE are weak. The maximum appears where the isopycnal temperature gradient is small, and float dispersion across temperature contours becomes larger, in spite of the weak EKE. In about 15% of the bins, κ^E is negative, implying that the eddy fluxes are directed up the mean isopycnal temperature gradient. The along-streamline averaged diffusivities are the result of large along-streamline variation of the differences and common features of both κ^L and κ^E.

Figures 10 and 11 show the depth–latitude comparison for two longitude bins. In bin 4 south of Australia (Fig. 10), there is one prominent jet around the latitude of 48°S, and both diffusivities show the tendency for a mixing barrier around 500 m and increased mixing with depth in the jet. Note, however, that κ^E is about double κ^L, and their respective maxima are located at different depths. Also, κ^L is large and positive at 500-m depth south of the jet, whereas κ^E is negative south of the jet, implying upgradient eddy temperature fluxes. Both κ^L and κ^E can be thought of as the product of two quantities [cf. Eqs. (2) and (5)]: a quantity that decreases with depth (the square root of the Lagrangian EKE, Fig. 10c, and the Eulerian eddy heat flux, Fig. 10d, respectively), and a quantity that increases with depth (the Lagrangian integral length scale, Fig. 10e, and the Eulerian reciprocal of the isopycnal temperature gradient, Fig. 10f, respectively). The cross-$\overline{\Theta}$ eddy heat flux (Fig. 10d) decreases more sharply than the eddy kinetic energy (Fig. 10c). The maximum in κ^E appears at depths where eddy heat flux is still large and isopycnal temperature gradients are starting to decrease. The Lagrangian integral length scale has a large maximum around 2000-m depth (Fig. 10e), approximately at the depth of the maximum in the reciprocal of the isopycnal temperature gradient (Fig. 10f). Both diffusivities show the mixing barrier effect in the upper 500 m in spite of the large Lagrangian eddy kinetic energy and Eulerian eddy heat flux.

The region upstream of the Drake Passage (Fig. 11) is an example of a region where the streamlines are farther apart, and the jets are not as distinct as in the region shown in Fig. 10 (cf. also Fig. 6). In these regions, the

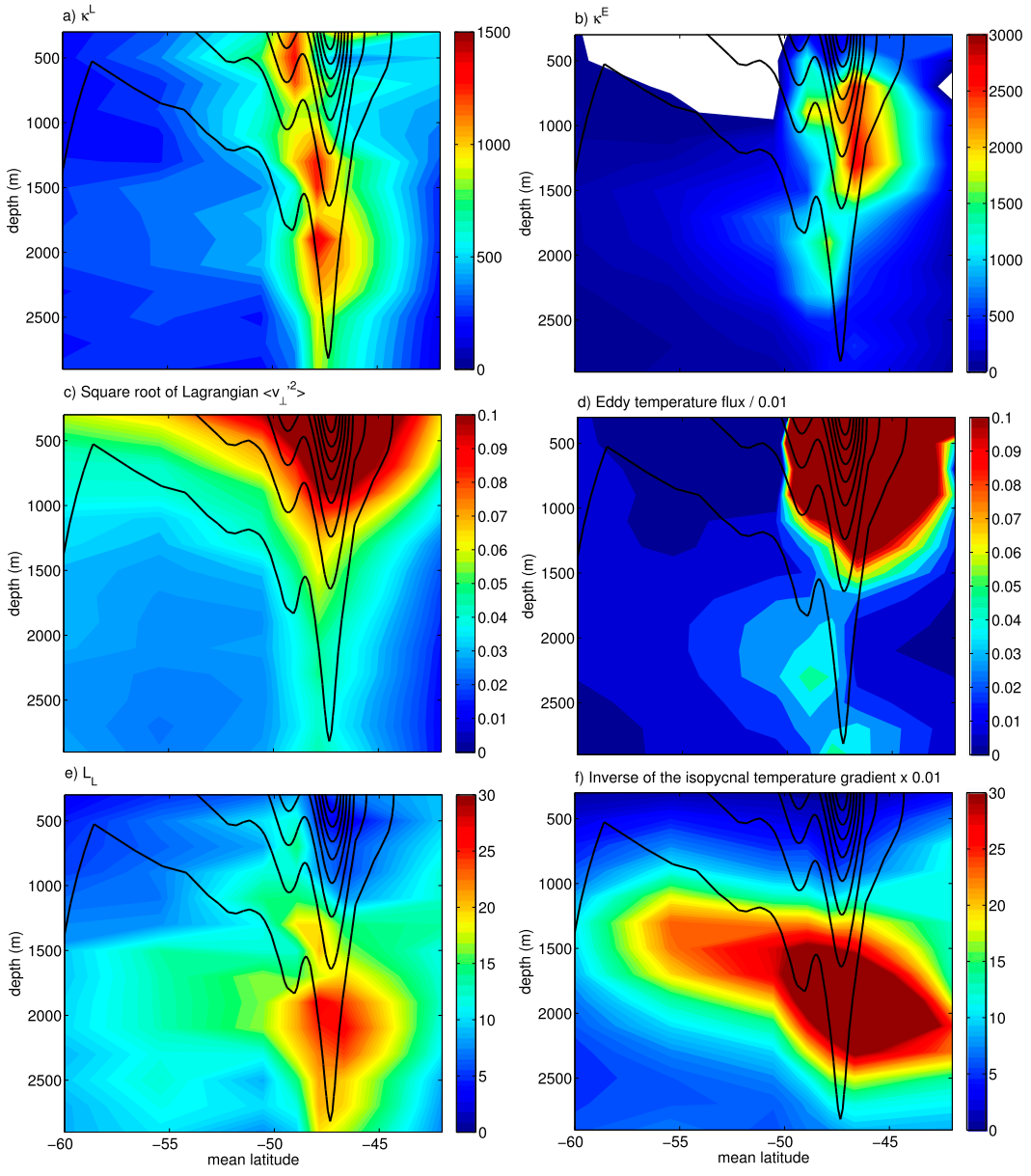

FIG. 10. Average over 120°–145°E, the western half of lon bin 4 from Fig. 6, corresponding to an average over two overlapping bins. (a) Lagrangian and (b) Eulerian diffusivities ($m^2\,s^{-1}$), (c) Lagrangian $\sqrt{\langle v_\perp'^2 \rangle}$ ($m\,s^{-1}$), (d) Eulerian eddy temperature flux divided by 0.01 ($m\,s^{-1}\,°C^{-1}$), (e) Lagrangian eddy integral scale (km), and (f) Eulerian reciprocal of the isopycnal temperature gradient times 0.01 ($m\,°C^{-1}$). The factor 0.01 was chosen to be able to better compare the vertical structure of Eulerian and Lagrangian quantities.

difference between the diffusivity above 500 m and below 500 m (Figs. 11a,b) is not as large as in the regions with more distinct jets (Figs. 10a,b). Both κ^E and κ^L show a broad maximum at around 1500–2000-m depth, a result of both the Lagrangian integral scale as well as the reciprocal of the isopycnal temperature gradient having a maximum at these depths (Figs. 11e,f). Here κ^L is about the same size above 500 m as it is below 1000 m, and the mixing barrier effect seems weaker than in the regions with more distinct jets. The difference between upper-ocean κ^E and κ^E below 1000 m is larger than for the Lagrangian diffusivity, but not as large as in Figs. 10a and 10b. The larger κ^L in the upper ocean may also be a result of the floats entering mixed layer regimes.

Figures 12b and 12c show the large longitudinal variability of κ^E and κ^L and their depth dependence, within the streamline bin indicated in Fig. 12a. Bins overlap by 5° longitude, so we do not resolve diffusivity differences

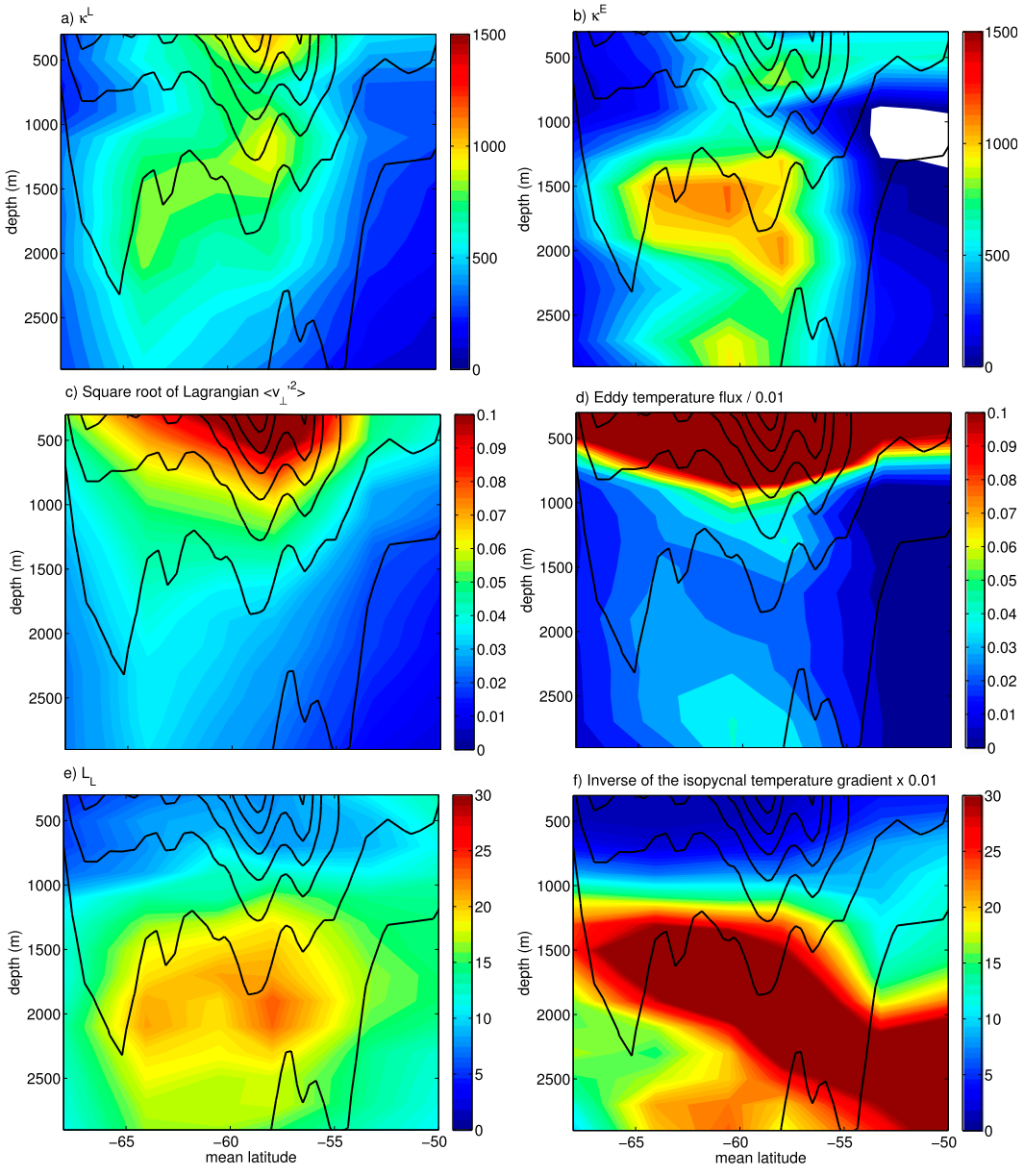

FIG. 11. Average over 240°–280°E, lon bin 7 from Fig. 6, corresponding to an average over five overlapping bins in lon. (a) Lagrangian and (b) Eulerian diffusivities ($m^2\,s^{-1}$), (c) Lagrangian $\sqrt{\langle v_\perp'^2 \rangle}$ ($m\,s^{-2}$), (d) Eulerian eddy heat flux divided by 0.01 ($m\,s^{-1}\,°C^{-1}$), (e) Lagrangian eddy integral scale (km), and (f) Eulerian reciprocal of the isopycnal temperature gradient times 0.01 ($m\,°C^{-1}$). The factor 0.01 was chosen to be able to better compare the vertical structure of Eulerian and Lagrangian quantities.

on scales smaller than this length. Judging from the fairly smooth distribution of quantities in Fig. 12, we conclude that no more information can be gained by decreasing the overlapping bin size. Figure 12a shows that the streamline bin encounters different dynamical regimes. While κ^E is generally larger than κ^L (note the different color scales in Figs. 12b,c), their depth dependences share some common features: close to the Agulhas region characterized by high surface eddy activity (see Figs. 12d,e), both κ^E and κ^L decrease from 500 m downward. To the east of the Kerguelen Plateau (centered around 51°S, 74°E), the streamline bin encounters a region with one prominent jet, extending from about 100° to 150°E. In this region, both κ^E and κ^L indicate mixing barriers at the surface and a steering level signature at depth. There are also, however, upgradient Eulerian eddy fluxes in the upper 500 m (Figs. 12c,e). After the flow has veered around topographic features, such as New Zealand

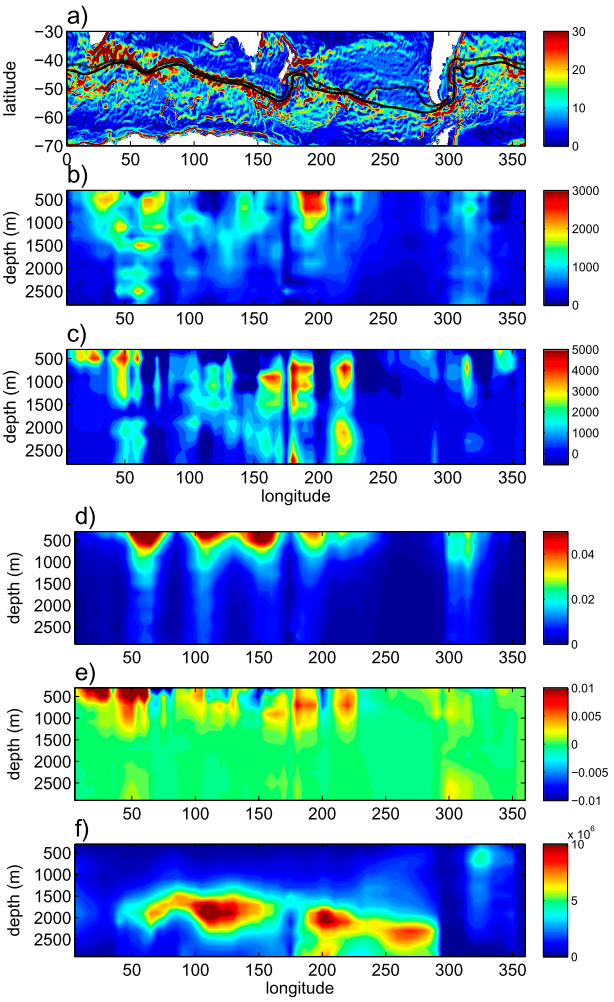

FIG. 12. (a) Along-streamline variation of quantities for the streamline bin shown together with the Eulerian mean velocity (color). (b) Lagrangian and (c) Eulerian diffusivities ($m^2 s^{-1}$). (d) Lagrangian $\langle v'^2 \rangle$ ($m^2 s^{-2}$). (e) Eulerian cross-temperature contours eddy heat flux ($°C\,m^{-1}\,s^{-1}$). (f) Reciprocal of Eulerian isopycnal temperature gradient ($°C\,m^{-1}$).

(Campbell Plateau, ~170°E) or the Drake Passage (290°E), both κ^E and κ^L tend to show elevated values over the whole water column. High Lagrangian eddy kinetic energy (Fig. 12d) is often, but not always, collocated with high Eulerian cross-$\overline{\Theta}$ heat flux (Fig. 12e). Large κ^E values below about 1500 m are associated with an increase in the reciprocal of the isopycnal temperature gradient (Fig. 12f).

4. Summary and conclusions

The aim of this study was to compare, in a consistent way, estimates of Lagrangian and Eulerian isopycnal diffusivities (κ^L and κ^E) in the Southern Ocean of an eddying model and to explore their relationship to the mean jets. The philosophy has been to choose bins large enough to minimize the rotational eddy components of flow, which should have no impact on net tracer transport. In the case of the Lagrangian diffusivities, sufficiently long time lags (equivalent to choosing large bins) are needed for the diffusivities to converge (Griesel et al. 2010). If this diffusive limit is reached, we also expected the Eulerian fluxes averaged over the bins to have a net downgradient component. The bin sizes were chosen such that floats stay in the bin an average of 30 days. This time scale reflects the minimum of 30 days the cross-stream diffusivity needs to converge to values that are not dependent on the averaging time scale.

The results can be summarized as follows:

1) It is possible to estimate the full Lagrangian isopycnal diffusivity tensor, at least for depth levels below about 300 m, by projecting the float velocities at each float point across the Eulerian mean velocity and by subtracting the Eulerian mean at each float location in the along-stream direction thereby isolating $u'_{\parallel}$. The along-stream diffusivity estimated in this way is about 6 times larger than the cross-stream diffusivity.
2) The Eulerian mean jets are in general nonzonal and nonparallel, and meridional dispersion is significantly different from cross-stream dispersion (not only in the along-streamline average). Even in the region west of the Drake Passage (longitude bin 7 from Fig. 6) where mean streamlines appear quasi zonal, the deviation of the individual jets from zonal orientation is significant: the diffusivity in the cross-velocity direction averaged over the jets in this region is $630 \pm 200\,m^2 s^{-1}$ at 500 m and $440 \pm 200\,m^2 s^{-1}$ at 1500 m. Meridional dispersion gives diffusivities of $1500 \pm 300\,m^2 s^{-1}$ at 500 m and $1200 \pm 400\,m^2 s^{-1}$ at 1500 m.
3) Along-streamline averages of κ^L and κ^E are similar in distribution, but there is no net downgradient flux in about 15% of the bins, and κ^E values below 500 m tend to be larger than κ^L values. The diffusivities are high toward the northern flanks of the ACC ($>1500\,m^2 s^{-1}$) and lower in the ACC in regions where there are distinct jets away from topography ($700–1000\,m^2 s^{-1}$). In contrast with the findings of Abernathey et al. (2010), there is no clear signature of a maximum below the core of the mean jet in the along-streamline average associated with a steering level.
4) There is large longitudinal variability in the diffusivities and in their relation to the mean flow. Even within typical longitude bins, a single streamline is not directly associated with a single jet. Because the jets are not aligned with streamlines and not circumpolar (see also, e.g., Thompson et al. 2010), this dilutes the effect of mixing barriers or steering levels

in the along-streamline average. In bins where the individual small-scale jets combine to form one larger prominent jet that is associated with a number of streamlines (notably between 80° and 160°E), the spatial distribution of diffusivities is as we might expect: mixing barriers at the surface in the jet, high diffusivities to the north and south of the jet, and a local maximum at depth below the jet. In bins where mean jets merge and diverge because of topography, there is no consistent relation of the diffusivities with the mean flow. Hence, no matter how jet-centric the definition of the bins, because the scale of the jets is smaller than the bin size (because of the need for long enough time lags), one bin may represent an average over multiple jets with locally different eddy–mean flow interaction characteristics. Notably, in the region west of the Drake Passage where the mean flow is broader and weaker, Lagrangian diffusivities are more uniform with depth as compared to the regions with distinct jets. This region has been of particular interest to the Diapycnal and Isopycnal Mixing Experiment in the Southern Ocean (DIMES; Gille et al. 2012). Recently, Tulloch et al. (2013, manuscript submitted to *J. Phys. Oceanogr.*) provided the first direct estimates of isopycnal eddy diffusivity from tracer observations, made as part of DIMES, aided by the analyses of tracer dispersion in a numerical model for this region. Our findings for this region are similar to the Tulloch et al. (2013, manuscript submitted to *J. Phys. Oceanogr.*) results in that both κ^L and κ^E exhibit a local maximum below depths of about 1000 m. Tulloch et al. (2013, manuscript submitted to *J. Phys. Oceanogr.*) interpreted this maximum as a steering level signature. At a depth of 1500 m, our model results show $\kappa^E = 1130 \pm 151\,\mathrm{m^2\,s^{-1}}$, $\kappa^L_{\mathrm{EM}} = 777 \pm 257\,\mathrm{m^2\,s^{-1}}$, $\kappa^L_{\mathrm{TM}} = 836 \pm 221\,\mathrm{m^2\,s^{-1}}$, while Tulloch et al. (2013, manuscript submitted to *J. Phys. Oceanogr.*) report $710 \pm 260\,\mathrm{m^2\,s^{-1}}$ at 1500 m from the observational estimate. The subscripts "EM" and "TM" refer to the projection of the Lagrangian velocity across the Eularian mean velocity and the mean potential temperature contours, respectively. The finding that a clear steering signature at depth, and mixing barriers at the surface, can most prominently be found in regions away from topography with distinct jets also seems consistent with the ideas presented in Sallée et al. (2011) who found that surface diffusivities are enhanced in the wake of large topographic obstacles where the mixing barrier effect can break down.

5) In theory, if the diffusive limit is reached in the Lagrangian diffusivity, then the Eulerian isopycnal eddy tracer fluxes, averaged over the same bins, should be representable as a diffusive parameterization with the Lagrangian diffusivities. In about 15% of the bins, the Eulerian isopycnal eddy fluxes are upgradient. Investigating the coherence of the eddy tracer flux with the mean tracer gradients, Griesel et al. (2009) found that for depth levels below the surface, more than 40% of the total eddy heat flux can be represented as a diffusive downgradient process when fields are filtered in space over length scales of at least 40°, but there was no significant coherence for scales smaller than about 40°. This is not inconsistent with the requirement of the bin size of 20° proposed here. However, Griesel et al. (2009) also concluded that the eddy flux is dominated by rotational components at all scales. We have attempted to explain, at least in a qualitative manner, the differences in the spatial distribution of Eulerian and Lagrangian diffusivities. Eddy kinetic energy and heat transport generally both strongly decrease with depth. In contrast, the Lagrangian integral length scale as well as the inverse of the temperature gradient increase with depth (the former because of multiple negative lobes in the AC in the upper ocean and the latter because the isopycnal temperature gradient decreases with depth). Differences in Eulerian and Lagrangian diffusivity distributions arise because the maxima and minima of the Lagrangian eddy kinetic energy are not always collocated with the maxima and minima in the Eulerian eddy fluxes. Eulerian diffusivities are negative in 15% of the bins. That the Eulerian diffusivities as determined here from the cross-contour eddy heat flux and the Lagrangian diffusivities differ may not be surprising: Lagrangian diffusivity is more like a potential vorticity diffusivity (Vollmer and Eden 2013; Abernathey et al. 2013) that in practice can differ from isopycnal temperature diffusion.
6) Finally, the isopycnal diffusivities diagnosed here are to be distinguished from the coefficients used in the GM parameterization that account for eddy-driven advection and may be dynamically more relevant (e.g., Griesel and Morales Maqueda 2006; Marshall and Radko 2006; Viebahn and Eden 2010). Because the GM diffusivities are diagnosed from the horizontal buoyancy gradients, which differ from the isopycnal tracer gradients, they may have different vertical distributions as found, for example, in Vollmer and Eden (2013), Smith and Marshall (2009), and Abernathey et al. (2013). The exploration of that issue is left for future work.

Acknowledgments. This work was funded by NSF Grant OCE0960914. Thanks to Mathew Maltrud (LANL) for providing his tripole POP setup and grid, initial

condition and forcing, and for helping with the float deployments. This research was supported by an allocation of advanced computing resources OCE960914 provided by the National Science Foundation. The computations were performed on Kraken at the National Institute for Computational Sciences (http://www.nics.tennessee.edu/). JLM was also supported by the Office of Science (BER), U.S. Department of Energy under DE-GF0205ER64119 and a Los Alamos National Laboratory subcontract.

REFERENCES

Abernathey, R., and J. Marshall, 2013: Global surface eddy diffusivities derived from satellite altimetry. *J. Geophys. Res. Oceans,* **118,** 901–916, doi:10.1002/jgrc.2006.

——, ——, M. Mazloff, and E. Shuckburgh, 2010: Enhanced isopycnal mixing at steering levels in the Southern Ocean. *J. Phys. Oceanogr.,* **40,** 170–184.

——, D. Ferreira, and A. Klocker, 2013: Diagnostics of eddy mixing in a circumpolar channel. *Ocean Modell.,* **72,** 1–16.

Bauer, S., M. S. Swenson, A. Griffa, A. J. Mariano, and K. Owens, 1998: Eddy–mean flow decomposition and eddy–diffusivity estimates in the tropical Pacific Ocean: 1. Methodology. *J. Geophys. Res.,* **103** (C13), 30 855–30 871.

Berloff, P. S., and J. C. McWilliams, 2002a: Material transport in oceanic gyres. Part I: Phenomenology. *J. Phys. Oceanogr.,* **32,** 764–796.

——, and ——, 2002b: Material transport in oceanic gyres. Part II: Hierarchy of stochastic models. *J. Phys. Oceanogr.,* **32,** 797–830.

Bower, A. S., H. T. Rossby, and J. L. Lillibridge, 1985: The Gulf Stream—Barrier or blender? *J. Phys. Oceanogr.,* **15,** 24–32.

Chelton, D. B., M. G. Schlax, R. M. Samelson, and R. A. deSzoeke, 2007: Global observations of large oceanic eddies. *Geophys. Res. Lett.,* **34,** L15606, doi:10.1029/2007GL030812.

——, ——, and ——, 2011: Global observations of nonlinear mesoscale eddies. *Prog. Oceanogr.,* **91,** 167–216.

Davis, R., 1987: Modelling eddy transport of passive tracers. *J. Mar. Res.,* **45,** 635–666.

——, 1991: Observing the general circulation with floats. *Deep-Sea Res.,* **38** (Suppl.), S531–S571.

——, 2005: Intermediate-depth circulation of the Indian and South Pacific Oceans measured by autonomous floats. *J. Phys. Oceanogr.,* **35,** 683–707.

Eden, C., 2006: Thickness diffusivity in the Southern Ocean. *Geophys. Res. Lett.,* **33,** L11606, doi:10.1029/2006GL026157.

——, R. J. Greatbatch, and D. Olbers, 2007a: Interpreting eddy fluxes. *J. Phys. Oceanogr.,* **37,** 1282–1296.

——, ——, and J. Willebrand, 2007b: A diagnosis of thickness fluxes in an eddy-resolving model. *J. Phys. Oceanogr.,* **37,** 727–742.

Ferrari, R., and M. Nikurashin, 2010: Suppression of eddy mixing across jets in the Southern Ocean. *J. Phys. Oceanogr.,* **40,** 1501–1519.

Ferreira, D., J. Marshall, and P. Heimbach, 2005: Estimating eddy stresses by fitting dynamics to observations using a residual-mean ocean circulation model and its adjoint. *J. Phys. Oceanogr.,* **35,** 1891–1910.

Gent, P. R., and J. C. McWilliams, 1990: Isopycnal mixing in ocean circulation models. *J. Phys. Oceanogr.,* **20,** 150–155.

Gille, S. T., and Coauthors, 2012: The diapycnal and isopycnal mixing experiment: A first assessment. *CLIVAR Exchanges,* No. 17, International CLIVAR Project Office, Southampton, United Kingdom, 46–48.

Green, J. S., 1970: Transfer properties of the large-scale eddies and the general circulation of the atmosphere. *Quart. J. Roy. Meteor. Soc.,* **96,** 157–185.

Griesel, A., and M. A. Morales Maqueda, 2006: The relation of meridional pressure gradients to North Atlantic Deep Water volume transport in an ocean general circulation model. *Climate Dyn.,* **26,** 781–799.

——, S. T. Gille, J. Sprintall, J. L. McClean, and M. E. Maltrud, 2009: Assessing eddy heat flux and its parameterization: A wavenumber perspective from a 1/10° ocean simulation. *Ocean Modell.,* **29,** 248–260, doi:10.1016/j.ocemod.2009.05.004, 248–260.

——, ——, ——, ——, J. H. LaCasce, and M. E. Maltrud, 2010: Isopycnal diffusivities in the Antarctic Circumpolar Current inferred from Lagrangian floats in an eddying model. *J. Geophys. Res.,* **115,** C06006, doi:10.1029/2009JC005.

Griffies, S. M., 1998: The Gent–McWilliams skew flux. *J. Phys. Oceanogr.,* **28,** 831–841.

Hurrell, J. W., J. J. Hack, D. Shea, J. M. Caron, and J. Rosinski, 2008: A new sea surface temperature and sea ice boundary data set for the community atmosphere model. *J. Climate,* **21,** 5145–5153.

Klocker, A., R. Ferrari, and J. H. LaCasce, 2012a: Estimating suppression of eddy mixing by mean flows. *J. Phys. Oceanogr.,* **42,** 1566–1576.

——, ——, ——, and S. T. Merrifield, 2012b: Reconciling float-based and tracer-based estimates of eddy diffusivities. *J. Mar. Res.,* **70,** 569–602.

Koszalka, I., J. H. LaCasce, M. Andersson, K. A. Orvik, and C. Mauritzen, 2011: Surface circulation in the Nordic seas from clustered drifters. *Deep-Sea Res.,* **58,** 468–485.

Krauss, W., and C. Böning, 1987: Lagrangian properties of eddy fields in the northern North Atlantic as deduced from satellite-tracked buoys. *J. Mar. Res.,* **45,** 259–291.

LaCasce, J. H., 2000: Floats and *f*/*H*. *J. Mar. Res.,* **58,** 61–95.

——, 2008: Lagrangian statistics from oceanic and atmospheric observations. *Transport and Mixing in Geophysical Flows,* J. B. Weiss and A. Provenzale, Eds., Springer, 165–218.

Large, W. G., and S. Pond, 1982: Sensible and latent heat flux measurements over the oceans. *J. Phys. Oceanogr.,* **12,** 464–482.

——, and S. G. Yeager, 2009: The global climatology of an interannually varying air–sea flux data set. *Climate Dyn.,* **33,** 341–364.

Ledwell, J. R., and A. J. Watson, 1991: The Santa Monica Basin tracer experiment: A study of diapycnal and isopycnal mixing. *J. Geophys. Res.,* **96** (C5), 8695–8718.

Lumpkin, R., A.-M. Treguier, and K. Speer, 2002: Lagrangian eddy scales in the Northern Atlantic Ocean. *J. Phys. Oceanogr.,* **32,** 2425–2440.

Maltrud, M. E., and J. L. McClean, 2005: An eddy resolving global 1/10° ocean simulation. *Ocean Modell.,* **8,** 31–54.

——, F. Bryan, and S. Peacock, 2010: Boundary impulse response functions in a century-long eddying global ocean simulation. *Environ. Fluid Mech.,* **10,** 275–295, doi:10.1007/s10652-009-9154-3.

Marshall, J., and G. Shutts, 1981: A note on rotational and divergent eddy fluxes. *J. Phys. Oceanogr.,* **11,** 1677–1680.

——, and T. Radko, 2006: Residual-mean solutions for the Antarctic Circumpolar Current and its associated thermohaline circulation. *J. Phys. Oceanogr.,* **36,** 1806–1821.

——, E. Shuckburgh, H. Jones, and C. Hill, 2006: Estimates and implications of surface eddy diffusivity in the Southern Ocean

derived from tracer transport. *J. Phys. Oceanogr.,* **36,** 1806–1821.

Nakamura, N., 2001: A new look at eddy diffusivity as a mixing diagnostic. *J. Atmos. Sci.,* **58,** 3685–3702.

Naveira Garabato, A. C., R. Ferrari, and K. L. Polzin, 2011: Eddy stirring in the Southern Ocean. *J. Geophys. Res.,* **116,** C09019, doi:10.1029/2010JC006818.

Oh, S. I., V. Zhurbas, and W. S. Park, 2000: Estimating horizontal diffusivity in the East Sea (Sea of Japan) and the northwest Pacific from satellite-tracked drifter data. *J. Geophys. Res.,* **105** (C3), 6483–6492.

Riha, S., and C. Eden, 2011: Lagrangian and Eulerian lateral diffusivities in zonal jets. *Ocean Modell.,* **39,** 114–124.

Sallée, J. B., K. Speer, R. Morrow, and R. Lumpkin, 2008: An estimate of Lagrangian eddy statistics and diffusion in the mixed layer of the Southern Ocean. *J. Mar. Res.,* **66,** 441–463.

——, ——, and S. R. Rintoul, 2011: Mean-flow and topographic control on surface eddy-mixing in the Southern Ocean. *J. Mar. Res.,* **69,** 753–777.

Shuckburgh, E., H. Jones, J. Marshall, and C. Hill, 2009a: Robustness of effective diffusivity diagnostic in oceanic flows. *J. Phys. Oceanogr.,* **39,** 1993–2009.

——, ——, ——, and ——, 2009b: Understanding the regional variability of eddy diffusivity in the Pacific sector of the Southern Ocean. *J. Phys. Oceanogr.,* **39,** 2011–2023.

Smith, K., and J. Marshall, 2009: Evidence for deep eddy mixing in the Southern Ocean. *J. Phys. Oceanogr.,* **39,** 50–69.

Sokolov, S., and S. R. Rintoul, 2009: Circumpolar structure and distribution of the Antarctic Circumpolar Current fronts: 1. Mean circumpolar paths. *J. Geophys. Res.,* **114,** C11018, doi:10.1029/2008JC005108.

Taylor, G. I., 1921: Diffusion by continuous movements. *Proc. Roy. Soc. London,* **64A,** 476–490.

Thompson, A. F., and J. B. Sallée, 2012: Jets and topography: Jet transitions and the impact on transport in the Antarctic Circumpolar Current. *J. Phys. Oceanogr.,* **42,** 956–972.

——, P. H. Haynes, C. Wilson, and K. J. Richards, 2010: Rapid Southern Ocean front transitions in an eddy-resolving ocean GCM. *Geophys. Res. Lett.,* **37,** L23602, doi:10.1029/2010GL045386.

Veneziani, M., A. Griffa, A. M. Reynolds, and A. J. Mariano, 2004: Oceanic turbulence and stochastic models from subsurface Lagrangian data for the Northwest Atlantic Ocean. *J. Phys. Oceanogr.,* **34,** 1884–1906.

——, ——, ——, Z. D. Garraffo, and E. P. Chassignet, 2005: Parameterizations of Lagrangian spin statistics and particle dispersion in presence of coherent vortices. *J. Mar. Res.,* **63,** 1057–1083.

Viebahn, J., and C. Eden, 2010: Towards the impact of eddies on the response of the Southern Ocean to climate change. *Ocean Modell.,* **34,** 150–165, doi:10.1016/j.ocemod.2010.05.005.

——, and ——, 2012: Standing eddies in the meridional overturning circulation. *J. Phys. Oceanogr.,* **42,** 1486–1508.

Vollmer, L., and C. Eden, 2013: A global map of meso-scale eddy diffusivities based on linear stability analysis. *Ocean Modell.,* **72,** 198–209.

Zhurbas, V., and S. I. Oh, 2004: Drifter-derived maps of lateral diffusivity in the Pacific and Atlantic Oceans in relation to surface circulation patterns. *J. Geophys. Res.,* **109,** C05015, doi:10.1029/2003JC002241.